NANO LETTERS

pubs.acs.org/NanoLett Letter

Steering Room-Temperature Plexcitonic Strong Coupling: A Diexcitonic Perspective

Wenbo Zhang, Jia-Bin You, Jingfeng Liu, Xiao Xiong, Zixian Li, Ching Eng Png, Lin Wu,* Cheng-Wei Qiu,* and Zhang-Kai Zhou*

Cite This: *Nano Lett.* 2021, 21, 8979−8986 Read Online

ACCESS | Metrics & More | Article Recommendations | Supporting Information

ABSTRACT: Plexcitonic strong coupling between a plasmon−polariton and a quantum emitter empowers ultrafast quantum manipulations in the nanoscale under ambient conditions. The main body of previous studies deals with homogeneous quantum emitters. To enable multiqubit states for future quantum computing and network, the strong coupling involving two excitons of the same material but different resonant energies has been investigated and observed primarily at very low temperature. Here, we report a room-temperature diexcitonic strong coupling (DiSC) nanosystem in which the excitons of a transition metal dichalcogenide monolayer and dye molecules are both strongly coupled to a single Au nanocube. Coherent information exchange in this DiSC nanosystem could be observed even when exciton energy detuning is about five times larger than the respective line widths. The strong coupling behaviors in such a DiSC nanosystem can be manipulated by tuning the plasmon resonant energies and the coupling strengths, opening up a paradigm of controlling plasmon-assisted coherent energy transfer.

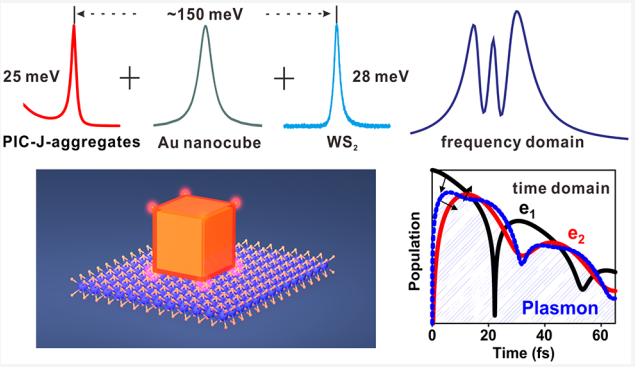

KEYWORDS: *Nano-optics, quantum plasmonics, plexcitonic strong coupling, full-quantum theory*

Strong coupling between quantum emitters (QEs) and photons can generate qubits that sustain coherent states enabling quantum information to be transmitted over a long distance or processed within an ultrafast time, which is essential for quantum communication and computing.[1−3] However, it is challenging to realize strong coupling at deep subwavelength scale (i.e., comparable to the scale of QEs) due to the difficulty of precise photon control and field confinement. With the flourish of cavity quantum electrodynamics (cQED), a variety of effective approaches have been proposed to push the interactions between QEs and photons to strong coupling regime. It not only deepens our understandings in fundamental quantum science[4−7] but also opens up possibilities for a number of advanced quantum devices.[8−11] The common feature of these approaches lies in the employment of cavities to reduce the effective mode volume V_{eff} for photons, so as to substantially increase the coupling strength g that is inversely proportional to $(V_{eff})^{1/2}$.[12] According to cQED theory, when g exceeds the damping rates of both the QE and cavity, the strong coupling between QEs and photons can be realized, which is characterized by the Rabi splitting (or oscillations) in frequency (or time) domain. Thanks to the advances of nanofabrication and theoretical developments, numerous nanocavities with ultrasmall V_{eff} have been proposed to realize strong coupling,[13−17] leading to various remarkable achievements, including the observation of Rabi splitting or oscillations,[18−20] room temperature strong coupling at the quantum optics limit,[21−23] and applications varying from physics[24] to electronics[25,26] and even chemistry.[27,28]

Beyond the realizations of strong coupling in various nanosystems, the quantum world still calls for further and deeper study. One of the primary objectives of studying strong coupling in cQED is to build quantum network by integrating numbers of qubits in which quantum states can be efficiently manipulated by photonic elements, leading to a large variety of scientific and technological frontiers, such as quantum secure communications and scalable quantum computing.[29,30] However, at present the majority of strong coupling works involve homogeneous QEs (from the same material and with resonant energies),[18−28] which are collectively considered as an ensemble, and these strong coupling systems only support two coherent states. On the other side with the fast

Received: June 9, 2021
Revised: October 7, 2021
Published: October 13, 2021

https://doi.org/10.1021/acs.nanolett.1c02248
Nano Lett. 2021, 21, 8979−8986

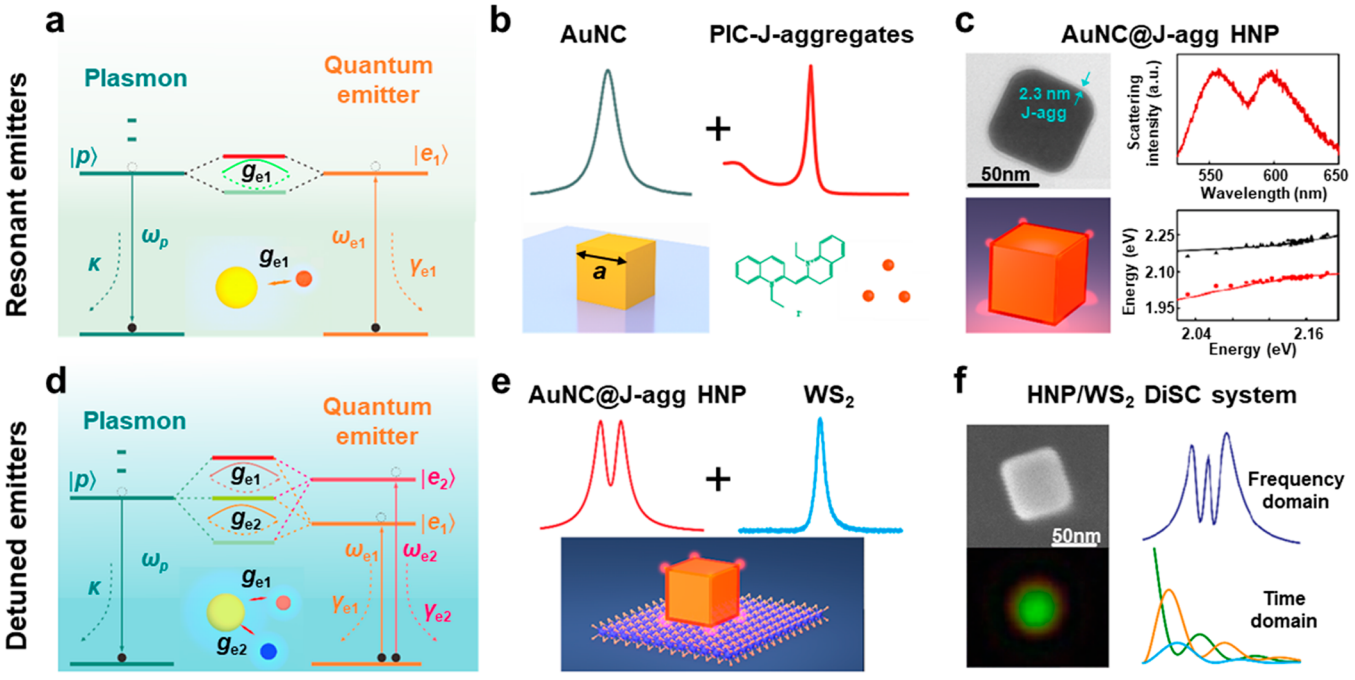

Figure 1. Schemes of strong coupling plexcitonic nanosystems with resonant emitters (upper) and detuned emitters (lower). (a,d) Energy level diagrams showing the couplings between plasmon and emitters: (a) the resonant emitter ensemble (e.g., single type of excitons) collectively represented by a single two-level system; (d) the detuned emitter ensemble (e.g., diexcitons) treated as two different two-level systems. (b,e) Representative constructions of the single-excitonic and diexcitonic strong coupling nanosystems: (b) AuNC coated with a layer of J-aggregates (AuNC@J-agg); (e) the AuNC@J-agg hybrid nanoparticle (HNP) sitting on WS_2 monolayer. (c,f) Optical characteristics of the respective nanosystems: (c) the experimentally measured scattering spectra showing Rabi splitting (top) and anticrossing (bottom); (f) the three-peak spectrum (top) and the temporal dynamics (bottom) for illustration purposes.

development of quantum science, besides the quantum dots (QDs) a large variety of promising QEs have been proposed for constructing strong coupling, such as the two-dimensional transition metal dichalcogenides (TMDC)[31−36] and carbon nanotubes.[37,38] The integration of heterogeneous QEs with arbitrary morphology and characteristics in the same quantum photonic platform seems ready to come out at one's call. Therefore, at this juncture the investigation of strong coupling of diexcitonic system is rapidly growing as an emerging research emphasis. For example, Qian et al. successfully realized two-photon Rabi splitting in a strongly coupled cavity-quantum-dot system consisting of a high-quality-factor photonic crystal cavity and intentionally grown InAs QDs with two exciton states.[39] In another work,[40] three bright intermixed plasmon−exciton−trion polariton states were observed from the strong interaction between localized surface plasmons in silver nanoprisms and excitons and trions in monolayer tungsten disulfide (WS_2). These pioneering diexcitonic works have employed different excitations in the same QE and successfully demonstrated three coherent states in a single nanoscale cavity, but the observations were generally made at low temperature (6−20 K) due to the properties of their selected QEs.

Inspired by these pioneering diexcitonic works, we construct a diexcitonic strong coupling (DiSC) nanosystem by integrating a TMDC monolayer with dye-molecules-coated Au nanocube (AuNC) and report its plexcitonic strong coupling behavior at room temperature. In particular, WS_2 and J-aggregates are selected for our first demonstration, where their excitons come from distinct materials with totally different morphologies and possess a large energy detuning (145 meV) about 5 times their respective line widths (~25 meV). Experimentally, we perform dark-field scattering measurements on the individual samples of AuNC@J-agg/WS_2 and study the anticrossing dispersion relationship of the DiSC nanosystem, which heavily depends on the properties of the constituting plasmon, excitons, and the coupling strength between them. We also demonstrate a proof of concept for the application of our DiSC nanosystem: plasmon-assisted coherent energy transfer between far-detuned QEs.

To construct a DiSC nanosystem, we start from a plexcitonic system that couples plasmon with single exciton. Here, the single exciton not only includes individual excitons but also can be an emitter ensemble that is resonant and spectrally indistinguishable. As shown in Figure 1a, a plexcitonic system for resonant emitters is simplified to an excitonic quantum emitter (e_1, a two-level system) with transition energy of ω_{e1} and decay rate of γ_{e1}, and a plasmon cavity with resonant energy of ω_p and decay rate of κ with coupling coefficient of g_{e1}. When g_{e1} is larger than both κ and γ_{e1}, two new coupled-states are generated in the system because of the coherent energy transfer between e_1 and plasmon. The two eigenstates can be spectrally observed as Rabi splitting, where the values of two spectral peaks correspond to the eigenvalues. The eigenvalues typically follow an anticrossing relationship, which can be obtained by tuning the optical spectral peaks as a function of the energy detuning between ω_{e1} and ω_p.[41]

In our experiment, as shown in Figure 1b, the resonant-emitter plexcitonic system is fabricated by coating AuNC (plasmon) with PIC-J-aggregates (e_1), and we defined it as the AuNC@J-agg hybrid nanoparticle (HNP). Detailed descriptions on the fabrication of AuNC@J-agg HNP are provided in Methods in Supporting Information. Taking a AuNC with side length of a = 68 nm as an example, we measured ω_p = 2145

https://doi.org/10.1021/acs.nanolett.1c02248
Nano Lett. 2021, 21, 8979−8986

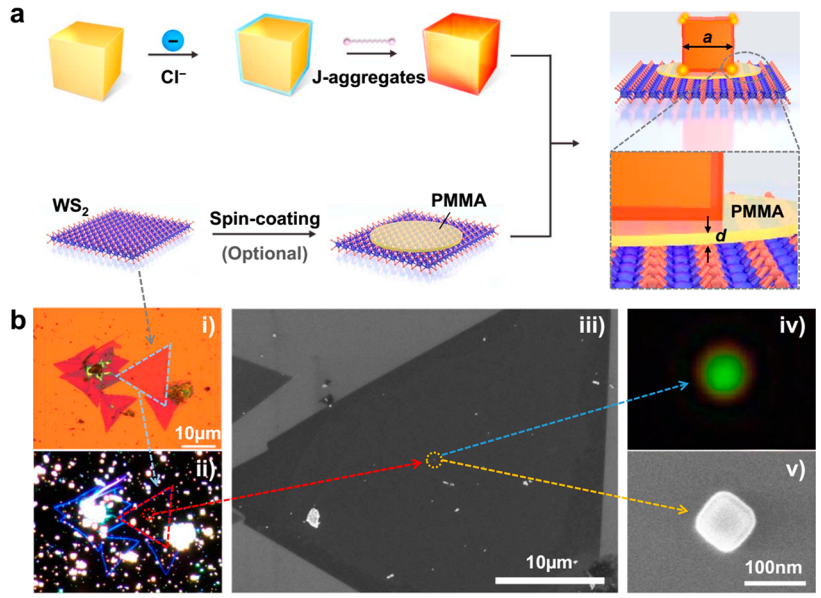

Figure 2. Fabrication and optical characterizations. (a) The fabrication process of the AuNC@J-agg/WS_2 DiSC nanosystem. (b) Optical characterizations: (i) bright- and (ii) dark-field images of WS_2 monolayer, (iii) low-magnification SEM, (iv) dark-field, and (v) high-magnification SEM images of a single AuNC@J-agg/WS_2 nanosystem.

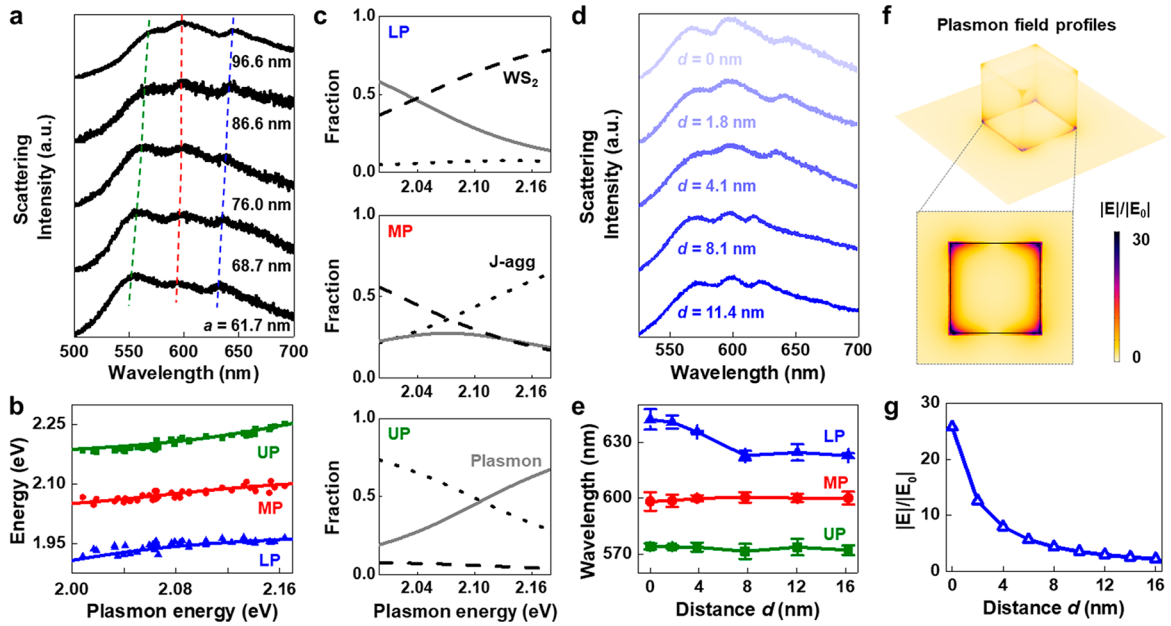

Figure 3. Manipulating the DiSC nanosystems with energy detunings and coupling strength engineering. (a) Scattering spectra of five representative individual AuNC@J-agg/WS_2 hybrids with varied sizes a = 60−100 nm. (b) Anticrossing dispersion relationship of all DiSC individuals with varied plasmon resonant energies, representing eigenvalues dependence on the energy detuning between exciton and plasmon. Green, blue, and red dots represent the experimental data of upper polariton (UP), middle polariton (MP), and lower polariton (LP), and the corresponding lines are theoretical fitting results. (c) Polariton branch mixing of WS_2 exciton (dashed line), J-aggregates exciton (dotted line), and plasmon (solid line) for LP, MP, and UP branches. (d) The coupling strength g_{e2} is tuned by varying the thickness of PMMA between the AuNC@J-agg HNP and the WS_2 monolayer d = 0−12 nm, resulting in different scattering spectra for the DiSC nanosystems. (e) The peak wavelengths for UP (green), MP (red), and LP (blue) branches as a function of the thickness of PMMA layer. (f) Numerical simulated plasmon field profiles of the AuNC@J-agg/WS_2 cavity when spacer thickness d = 0. Top: Three-dimensional profiles showing hotspots at all AuNC corners. Bottom: Profile at the interface between J-aggregates and WS_2. (g) The field enhancement at ω_{e2} at the WS_2 surface as a function of spacer thickness d.

meV and κ = 242 meV (extracted from dark-field scattering). The optical properties of J-aggregates are measured as ω_{e1} = 2145 meV and γ_{e1} = 25 meV (extracted from extinction spectra). Using the J-aggregates coating with a thickness of ∼2 nm, an obvious Rabi splitting in spectrum (Figure 1c) is obtained based on the single-particle dark-field scattering measurement. The coupling strength g_{e1} = 90 meV > $|\gamma_{e1} - \kappa|/4$ unambiguously demonstrates that this single-exciton plexcitonic nanosystem is in strong coupling regime. By measuring the scattering spectra for different ω_p (tuned via AuNC size), we observe clear anticrossing dispersion as shown in Figure 1c. More detailed results on the single-exciton strong

https://doi.org/10.1021/acs.nanolett.1c02248
Nano Lett. 2021, 21, 8979−8986

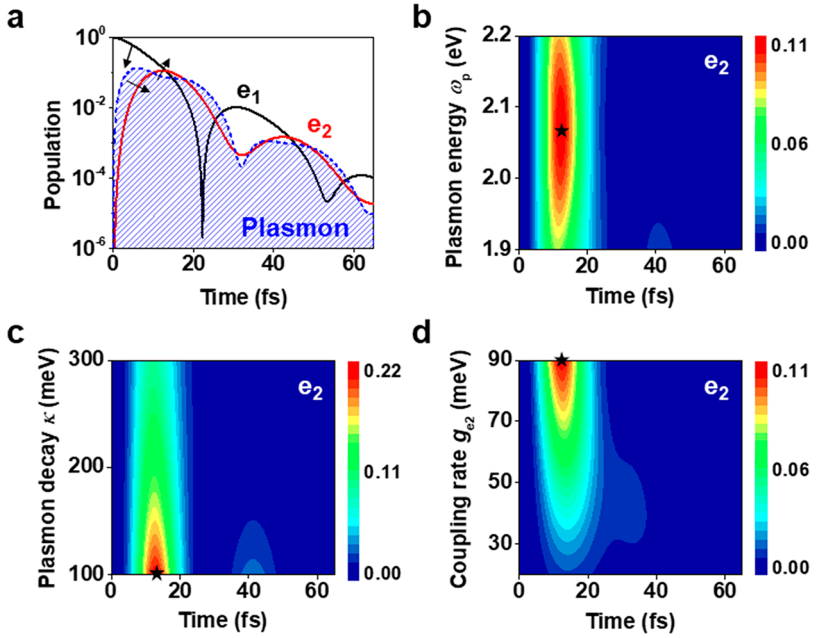

Figure 4. Plasmon-assisted energy transfer between detuned emitters e_1 (J-aggregates) and e_2 (WS_2). The intrinsic coupling between the detuned emitters is neglected, and e_1 is assumed initially excited with population of 1. (a) Time-dependent populations of the two emitters in a plasmonic cavity (ω_p = 2071 meV and κ = 242 meV), where the e_1 and e_2 are coupled to plasmonic cavity with coupling strength of g_{e1} = 90 meV and g_{e2} = 90 meV. (b–d) Tunable energy transfer process by varying the properties of plasmonic cavity: (b) resonant energy ω_p, (c) decay rate κ, and (d) coupling strength g_{e2} with e_2. Note that all parameters employed are within experimental reach. Stars represent the optimal parameters within the studied ranges.

coupling nanosystem can be found in Supporting Information (Figures S1 and S2).

Next, we introduce the second exciton e_2 with transition frequency of ω_{e2} ($\omega_{e1} \neq \omega_{e2}$), decay rate of γ_{e2}, and coupling strength of g_{e2} with the plasmon cavity. As shown in Figure 1d, plexcitonic system for detuned emitters now can be described with the Hamiltonian

$$\hat{H} = \hbar \begin{pmatrix} \omega_p - i\frac{\kappa}{2} & g_{e1} & g_{e2} \\ g_{e1} & \omega_{e1} - i\frac{\gamma_{e1}}{2} & 0 \\ g_{e2} & 0 & \omega_{e2} - i\frac{\gamma_{e2}}{2} \end{pmatrix} \quad (1)$$

where the coupling between the excitons e_1 and e_2 is neglected due to their strongly detuned resonances. By diagonalizing the Hamiltonian in eq 1, we are able to identify the new eigenstates and eigenvalues, which now become three spectral peaks as illustrated in Figure 1f.

Experimentally, as illustrated in Figures 1e and 2a, we constructed a AuNC@J-agg/WS_2 DiSC system by taking AuNC@J-agg HNP as a building block and transferring it onto the surface of monolayer WS_2 (see atomic force microscopy results in Figure S3). The results about strong coupling behaviors of monolayer WS_2 and bare AuNC are provided in Figure S4. Usually, it may be difficult to build a DiSC nanosystem due to the poor integratability of a strong coupling nanosystem. However, with an open nanocavity, that is, AuNC, the strong coupling nanosystem of HNP can be facially integrated with the monolayer WS_2, resulting in the DiSC nanosystem of AuNC@J-agg/WS_2. More importantly, the coupling strength between HNP and the monolayer WS_2 can be controlled by introducing an additional layer of poly(methyl methacrylate) (PMMA). The PMMA layer could be spin-coated on the top of WS_2 with its thickness tunable ranging from 0 to 12 nm with precision of ~1 nm (Figure S5). Figure 2b presents the images of our AuNC@J-agg/WS_2 sample obtained by dark-field setup and the scanning electronic microscopy (SEM). The monolayer WS_2 can be identified by both optical and SEM images (Figure 2b i–iii), and by comparing these images we are able to identify an individual HNP on the WS_2, that is, the AuNC@J-agg/WS_2, diexciton plexcitonic system. Before transferring AuNC@J-agg HNP, we measured the optical properties of WS_2, as ω_{e2} = 2000 meV and g_{e2} = 28 meV. Detailed information about bright-field and photoluminescence measurements of WS_2 can be found in Figure S3. In the following context, we shall dedicate our main effort in this work to study the optical characteristics of DiSC nanosystem in both frequency- and time-domains.

By performing dark-field scattering measurements for more than 100 individual AuNC@J-agg/WS_2 samples, the spectral evolution of the DiSC nanosystem is systematically studied. Detailed information about dark-field measurements can be found in Methods and Figure S6 in Supporting Information. Figure 3a displays the scattering spectra of five representative samples, where the three scattering peaks, corresponding to the three eigenvalues of the DiSC nanosystem, can be noted. By tuning the plasmon resonant energy ω_p via the size of AuNC (see Figure 2a and Figure S1), the anticrossing dispersion of the DiSC nanosystem is extracted from many individual AuNC@J-agg/WS_2 samples. As shown in Figure 3b, the symbols are experimental data obtained by reading the peaks in scattering spectra (Figure 3a). The three curves are theoretical fittings obtained by calculating the eigenvalues of eq 1 for diexciton plexcitonic system, and they correspond to the upper polariton (UP), middle polariton (MP) and lower polariton (LP) branches. Fitting results in the coupling strength of g_{e1} =

https://doi.org/10.1021/acs.nanolett.1c02248
Nano Lett. 2021, 21, 8979–8986

90 meV and g_{e2} = 90 meV, both of which satisfy the strong coupling condition of $g_{ei} > |\gamma_{ei} - \kappa|/4$ (i = 1, 2).

Diagonalization of the Hamiltonian in eq 1 yields the Hopfield coefficients (see Methods in Supporting Information for details),[42] which indicate the contribution fraction of plasmons, J-aggregates, and WS_2 to each polariton state. As illustrated in Figure 3c, the curves representing the contribution of plasmons, J-aggregates, and WS_2 are respectively marked by solid, dotted, and dashed lines. Clearly, LP is dominantly contributed by WS_2 coupling to plasmon, whereas UP is more relevant to the coupling between J-aggregates and plasmon. The presence of hybrid exciton−polariton states further confirms our realization of the DiSC nanosystem.

As the distance d between AuNC@J-agg HNP and monolayer WS_2 is tuned by the thickness of PMMA spacer, the coupling strength g_{e2} of our DiSC nanosystem can be manipulated. Figure 3d shows the representative spectra of individual DiSC nanosystems with different values of d (using different concentration of PMMA solution, see Figure S5). The statistical results of these spectral behaviors are presented in Figure 3e, which more vividly shows the dependence of the peak wavelength on d. One can see that as d increases from 0 to 16 nm, the LP resonant wavelength gradually drops from ∼641 nm and stays constant around 620 nm, which corresponds to the original exciton energy of monolayer WS_2 (2000 meV). This is reasonable as LP originates dominantly from the coupling between WS_2 and plasmon as suggested from Figure 3c. When d becomes larger than 8 nm, the exciton of WS_2 is effectively decoupled from the AuNC@J-agg HNP and becomes isolated. On the other hand, the MP and UP branches experience minor shifts with the increment of d, as the AuNC@J-agg HNP is kept almost unchanged throughout the process. In order to understand the role of plasmonic hotspots in altering the LP branch via spacer, we have also performed numerical simulations to study the field enhancements in the AuNC@J-agg/WS_2 nanosystem. Detailed descriptions on the simulation model and numerical results can be found in Supporting Information (Figure S7). As shown in Figure 3f, the AuNC possesses plasmonic hotspots at all corners (top) with higher enhancement at the interface with WS_2 (bottom). When the spacer thickness d increases, the field enhancement at the WS_2 surface below the cube corners quickly decreases, which explains the (de)coupling between AuNC@J-agg HNP and WS_2 and agrees well with the energy shift of LP in Figure 3e. This set of results in Figure 3 is particularly compelling in providing a way to actively couple or decouple one type of emitter, effectively switching between single-exciton and diexciton strong coupling plexcitonic nanosystems.

Upon demonstrating tunability of the plasmonic cavity and the coupling strength in our DiSC nanosystems, we are ready to venture into the plasmon-assisted energy transfer application. In Figure 4, we show our theoretical predictions on the plasmon-assisted energy transfer between emitters e_1 and e_2. All calculations are based on Lindblad master equation (see Methods in Supporting Information for details) and take the practical parameters extracted from our experiments: ω_{e1} = 2145 meV and γ_{e1} = 25 meV for e_1 (J-aggregates); ω_{e2} = 2000 meV and γ_{e2} = 28 meV for e_2 (WS_2). The time-dependent populations of photons and excitons can be obtained from an exponential of the diagonal eigenvalue matrix by a unitary transformation with the Hopfield coefficients (details can be found in Methods in Supporting Information). We assume that the intrinsic coupling between the excitons e_1 and e_2 in free space is negligible (i.e., $g_{e1\text{-}e2}$ = 0) due to their far-detuned resonances and e_1 is initially excited with a population of 1. When the two emitters are residing in a plasmonic cavity (ω_p = 2071 meV and κ = 242 meV) with coupling strength of g_{e1} = 90 meV and g_{e2} = 90 meV, we find with the assistance of the plasmonic cavity that the energy stored in e_1 can be transferred efficiently to e_2 as illustrated in Figure 4a. The energy is quickly passed within 10 fs from e_1 (black line) to plasmon (blue line), and then to e_2 (red line). Afterward, e_2 will oscillate coherently with the plasmon and simultaneously exchange energy with e_1.

We can optimize the design of the nanosystem to achieve a more efficient energy transfer. In Figure 4b, we study the effect of plasmon resonance on the energy transfer and find an optimal plasmon resonance ω_p= 2071 meV, which is in the middle between e_1 (ω_{e1} = 2145 meV) and e_2 (ω_{e2} = 2000 meV). The peaks of the large-detuned emitters and plasmon (detunings = 74 and 71 meV) spectrally overlap due to the relatively large decay rate of the plasmon (e.g., κ = 242 meV), leading to an efficient energy transfer between e_1/e_2 and plasmon. In Figure 4c,d, we study the effects of cavity decay rate κ and the coupling strength g_{e2} on the energy transfer. We find that the energy transfer will be further enhanced for smaller cavity decay and larger coupling strength. This is because a cavity with high quality factor can host more Rabi oscillations as well as coherent energy transfer within the coherent time. To optimize the energy transfer from e_1, in short we should adopt a "loss-less" plasmonic cavity that is best coupled to e_2 with the largest possible coupling strength and has a resonant energy in between e_1 and e_2. More interestingly, the energy transfer to e_2 could be actively tuned via varying the coupling rate g_{e2} by making use of the flexible substrate concept to apply pressure to PMMA spacer between the AuNC@J-agg HNP and WS_2 monolayer. Our results demonstrate an active control of coupling rates and open a new possibility to increase the coherent manipulations in quantum plasmonic devices.

In reality, it may not be true that the two detuned emitters are absolutely decoupled from each other, especially when they are in contact. We then studied the case where the two emitters exchange energies at a finite intrinsic coupling rate of $g_{e1\text{-}e2}$ = 10 meV (Figure S8) while keeping all of the other parameters unchanged from the case of Figure 4. It is clear that now the plasmon can enhance the energy transfer between the two emitters which are intrinsically coupled. The only difference lies in the optimized plasmon resonance, 1998 meV, which should be nearly resonant with e_2 (ω_{e2} = 2000 meV). Further discussions on the plasmonic-assisted energy transfer can be found in Supporting Information (Figure S9a,b).

In summary, we experimentally and theoretically investigated the strong coupling behaviors in a room-temperature DiSC AuNC@J-agg/WS_2 nanosystem, which was constructed by integrating a WS_2 monolayer with a J-aggregate-coated Au nanocube. The motivation originates from two aspects. First, the successful realization of strong coupling sequentially at low temperature,[4] room temperature,[18] and even at quantum limit under ambient conditions[22] has established a strong foundation toward exploring the applications of strong coupling, for example, quantum manipulation, entanglement, and integrated logic devices based on room-temperature strong coupling systems.[3,43] Second, various novel QEs including 2D

https://doi.org/10.1021/acs.nanolett.1c02248
Nano Lett. 2021, 21, 8979−8986

materials, perovskites, and carbon nanotubes have been proposed in constructing quantum devices,[44] which imply that the emerging hybrid quantum system with various kinds of QEs is inevitable[45−48] with the rapid growth of integrated quantum science. On the basis of these two aspects, we believe that it is the time to push the investigation of strong coupling to the era of DiSC.

There are two potential scenarios for investigating DiSC: spatially separated QEs with resonant frequency or detuned but closely spaced QEs. To investigate the first scenario on spatially separated QEs with resonant frequency, two major challenges should be overcome: (i) obtaining resonant QEs at room temperature, which might be more difficult than doing that at low temperature of a few Kelvin;[49,50] and (ii) locating two QEs precisely at their respective locations.[51,52] On the other hand, the study on the second scenario, DiSC nanosystems consisting of detuned but closely spaced QEs, also has plenty of room to investigate; for example, to identify the available energy detuning range of two excitons for a DiSC nanosystem and to understand the underlying quantum behaviors. In this work, we experimentally demonstrated that two excitons with energy detuning about 5 times larger than their line widths can simultaneously couple to a plasmonic nanocube strongly, exhibiting three coherent states at room temperature. Also, our full quantum mechanical time domain calculations indicated that the plasmonic cavity can assist the coherent energy transfer between the two far-detuned excitons, shortening the communicating time scale below 10 fs. Our further calculations also shows that the efficiency of plasmon-assisted energy transfer can be improved by increasing coupling strength, reducing the plasmon loss, and decreasing the energy detuning of two excitons (Figure S9c,d), suggesting guidelines for constructing DiSC in future. Looking forward, we believe that our work not only reveals the coupling behaviors of a DiSC nanosystem but also provides a platform with more degrees of freedom to study quantum mechanics and to inspire the design of future room-temperature quantum devices and quantum network.

■ ASSOCIATED CONTENT

Supporting Information

The Supporting Information is available free of charge at https://pubs.acs.org/doi/10.1021/acs.nanolett.1c02248.

Methods used in this manuscript; synthesized AuNCs and their tunable plasmon resonant modes; characterization of AuNC@J-agg HNP; characterization of monolayer WS_2; strong coupling of the AuNC/WS_2 hybrid; tunable thickness of PMMA layer; dark-field optical characterizations; effects of PMMA spacer thickness on the scattering and near-field for AuNC@J-agg/WS_2 nanosystems; plasmon-enhanced energy transfer between intrinsically coupled detuned emitters; the influences of plasmonic cavity's existence and emitter energy detuning on the energy transfer (PDF)

■ AUTHOR INFORMATION

Corresponding Authors

Lin Wu − *Institute of High Performance Computing, A*STAR (Agency for Science, Technology and Research), Connexis, Singapore 138632*; orcid.org/0000-0002-3188-0640; Email: wul@ihpc.a-star.edu.sg

Cheng-Wei Qiu − *Department of Electrical and Computer Engineering, National University of Singapore, Singapore 117583*; orcid.org/0000-0002-6605-500X; Email: eleqc@nus.edu.sg

Zhang-Kai Zhou − *State Key Laboratory of Optoelectronic Materials and Technologies, School of Physics, Sun Yat-sen University, Guangzhou 510275, China*; orcid.org/0000-0002-4341-3097; Email: zhouzhk@mail.sysu.edu.cn

Authors

Wenbo Zhang − *State Key Laboratory of Optoelectronic Materials and Technologies, School of Physics, Sun Yat-sen University, Guangzhou 510275, China*

Jia-Bin You − *Institute of High Performance Computing, A*STAR (Agency for Science, Technology and Research), Connexis, Singapore 138632*

Jingfeng Liu − *College of Electronic Engineering, South China Agricultural University, Guangzhou 510642, China*

Xiao Xiong − *Institute of High Performance Computing, A*STAR (Agency for Science, Technology and Research), Connexis, Singapore 138632*; orcid.org/0000-0002-7153-8081

Zixian Li − *State Key Laboratory of Optoelectronic Materials and Technologies, School of Physics, Sun Yat-sen University, Guangzhou 510275, China*

Ching Eng Png − *Institute of High Performance Computing, A*STAR (Agency for Science, Technology and Research), Connexis, Singapore 138632*

Complete contact information is available at: https://pubs.acs.org/10.1021/acs.nanolett.1c02248

Author Contributions

W.Z. and J.B.Y. contributed equally to this work. Z.K.Z. conceived the idea. Z.K.Z., L.W., and C.W.Q. supervised the project. W.Z performed the sample fabrication and characterizations. W.Z. and Z.L. carried out the optical measurements. J.B.Y., J.L., X.X., and C.E.P. conducted the theoretical analysis. Z.K.Z., L.W., and C.W.Q. cowrote the manuscript. All the authors discussed the results.

Notes

The authors declare no competing financial interest.

■ ACKNOWLEDGMENTS

This work was partially supported by the Key-Area Research and Development Program of Guangdong Province (2018B30329001), National Natural Science Foundation of China (11974437, 91750207), the Guangdong Special Support Program (2017TQ04C487, 2019JC0X397), Guangdong Natural Science Foundation (2020A0505140004), Open Fund of IPOC (BUPT) under Grant IPOC2019A003, and Fundamental Research Funds for the Central Universities, Sun Yat-sen University (20lgzd30). The IHPC team acknowledges the financial support from National Research Foundation Singapore (QEP-SF1) and A*STAR Career Development Award (SC23/21-8007EP). All authors gratefully acknowledge National Research Foundation (NRF) Singapore and the National Natural Science Foundation of China (NSFC) Joint Grant NRF2017NRF-NSFC002-015.

■ REFERENCES

(1) De Leon, N. P.; Lukin, M. D.; Park, H. Quantum Plasmonic Circuits. *IEEE J. Sel. Top. Quantum Electron.* **2012**, *18*, 1781−1791.

(2) Tame, M. S.; McEnery, K.; Özdemir, S.; Lee, J.; Maier, S. A.; Kim, M. Quantum Plasmonics. *Nat. Phys.* **2013**, *9*, 329−340.
(3) Xu, D.; Xiong, X.; Wu, L.; Ren, X.-F.; Png, C. E.; Guo, G.-C.; Gong, Q.; Xiao, Y.-F. Quantum Plasmonics: New Opportunity in Fundamental and Applied Photonics. *Adv. Opt. Photonics* **2018**, *10*, 703−756.
(4) Khitrova, G.; Gibbs, H.; Kira, M.; Koch, S. W.; Scherer, A. Vacuum Rabi Splitting in Semiconductors. *Nat. Phys.* **2006**, *2*, 81−90.
(5) Jacob, Z.; Shalaev, V. M. Plasmonics Goes Quantum. *Science* **2011**, *334*, 463−464.
(6) Jiang, X.; Shao, L.; Zhang, S.-X.; Yi, X.; Wiersig, J.; Wang, L.; Gong, Q.; Lončar, M.; Yang, L.; Xiao, Y.-F. Chaos-Assisted Broadband Momentum Transformation in Optical Microresonators. *Science* **2017**, *358*, 344−347.
(7) Ren, J.; Gu, Y.; Zhao, D.; Zhang, F.; Zhang, T.; Gong, Q. Evanescent-Vacuum-Enhanced Photon-Exciton Coupling and Fluorescence Collection. *Phys. Rev. Lett.* **2017**, *118*, 073604.
(8) Kolaric, B.; Maes, B.; Clays, K.; Durt, T.; Caudano, Y. Strong Light-Matter Coupling as a New tool for Molecular and Material Engineering: Quantum Approach. *Adv. Quant. Technol.* **2018**, *1*, 1800001.
(9) Fernández-Domínguez, A. I.; García-Vidal, F. J.; Martín-Moreno, L. Unrelenting Plasmons. *Nat. Photonics* **2017**, *11*, 8−10.
(10) Vasista, A. B.; Barnes, W. L. Molecular Monlayer Strong Coupling in Dielectric Soft Microcavities. *Nano Lett.* **2020**, *20*, 1766−1773.
(11) Wang, J.; Su, R.; Xing, J.; Bao, D.; Diederichs, C.; Liu, S.; Liew, T. C.; Chen, Z.; Xiong, Q. Room Temperature Coherently Coupled Exciton-Polaritons in Two-Dimensional Organic-Inorganic Perovskite. *ACS Nano* **2018**, *12*, 8382−8389.
(12) Kimble, H. J. The Quantum Internet. *Nature* **2008**, *453*, 1023−1030.
(13) Zhang, Y.; Meng, Q.-S.; Zhang, L.; Luo, Y.; Yu, Y.-J.; Yang, B.; Zhang, Y.; Esteban, R.; Aizpurua, J.; Luo, Y.; Yang, J.-L.; Dong, Z.-C.; Hou, J G Sub-Nanometre Control of the Coherent Interaction between a Single Molecule and a Plasmonic Nanocavity. *Nat. Commun.* **2017**, *8*, 1−7.
(14) Urbieta, M.; Barbry, M.; Zhang, Y.; Koval, P.; Sánchez-Portal, D.; Zabala, N.; Aizpurua, J. Atomic-Scale Lightning Rod Effect in Plasmonic Picocavities: a Classical View to a Quantum Effect. *ACS Nano* **2018**, *12*, 585−595.
(15) Kongsuwan, N.; Demetriadou, A.; Chikkaraddy, R.; Benz, F.; Turek, V. A.; Keyser, U. F.; Baumberg, J. J.; Hess, O. Suppressed Quenching and Strong-Coupling of Purcell-Enhanced Single-Molecule Emission in Plasmonic Nanocavities. *ACS Photonics* **2018**, *5*, 186−191.
(16) Ojambati, O. S.; Chikkaraddy, R.; Deacon, W. M.; Huang, J.; Wright, D.; Baumberg, J. J. Efficient Generation of Two-Photon Excited Phosphorescence from Molecules in Plasmonic Nanocavities. *Nano Lett.* **2020**, *20*, 4653−4658.
(17) Neuman, T.; Esteban, R.; Casanova, D.; García-Vidal, F. J.; Aizpurua, J. Coupling of Molecular Emitters and Plasmonic Cavities beyond the Point-Dipole Approximation. *Nano Lett.* **2018**, *18*, 2358−2364.
(18) Vasa, P.; Wang, W.; Pomraenke, R.; Lammers, M.; Maiuri, M.; Manzoni, C.; Cerullo, G.; Lienau, C. Real-Time Observation of Ultrafast Rabi Oscillations between Excitons and Plasmons in Metal Nanostructures with J-aggregates. *Nat. Photonics* **2013**, *7*, 128−132.
(19) Melnikau, D.; Esteban, R.; Savateeva, D.; Sánchez-Iglesias, A.; Grzelczak, M.; Schmidt, M. K.; Liz-Marzan, L. M.; Aizpurua, J.; Rakovich, Y. P. Rabi Splitting in Photoluminescence Spectra of Hybrid Systems of Gold Nanorods and J-aggregates. *J. Phys. Chem. Lett.* **2016**, *7*, 354−362.
(20) Wersall, M.; Cuadra, J.; Antosiewicz, T. J.; Balci, S.; Shegai, T. Observation of Mode Splitting in Photoluminescence of Individual Plasmonic Nanoparticles Strongly Coupled to Molecular Excitons. *Nano Lett.* **2017**, *17*, 551−558.
(21) Chikkaraddy, R.; De Nijs, B.; Benz, F.; Barrow, S. J.; Scherman, O. A.; Rosta, E.; Demetriadou, A.; Fox, P.; Hess, O.; Baumberg, J. J. Single-Molecule Strong Coupling at Room Temperature in Plasmonic Nanocavities. *Nature* **2016**, *535*, 127−130.
(22) Liu, R.; Zhou, Z.-K.; Yu, Y.-C.; Zhang, T.; Wang, H.; Liu, G.; Wei, Y.; Chen, H.; Wang, X.-H. Strong Light-Matter Interactions in Single Open Plasmonic Nanocavities at the Quantum Optics Limit. *Phys. Rev. Lett.* **2017**, *118*, 237401.
(23) Santhosh, K.; Bitton, O.; Chuntonov, L.; Haran, G. Vacuum Rabi Splitting in a Plasmonic Cavity at the Single Quantum Emitter limit. *Nat. Commun.* **2016**, *7*, 1−5.
(24) Peng, P.; Liu, Y. C.; Xu, D.; Cao, Q. T.; Lu, G.; Gong, Q.; Xiao, Y. F.; et al. Enhancing Coherent Light-Matter Interactions through Microcavity-Engineered Plasmonic Resonances. *Phys. Rev. Lett.* **2017**, *119*, 233901.
(25) Kongsuwan, N.; Demetriadou, A.; Chikkaraddy, R.; Baumberg, J. J.; Hess, O. Fluorescence Enhancement and Strong-Coupling in Faceted Plasmonic Nanocavities. *EPJ. Appl. Metamater.* **2018**, *5*, 6.
(26) Demetriadou, A.; Hamm, J. M.; Luo, Y.; Pendry, J. B.; Baumberg, J. J.; Hess, O. Spatiotemporal Dynamics and Control of Strong Coupling in Plasmonic Nanocavities. *ACS Photonics* **2017**, *4*, 2410−2418.
(27) Flick, J.; Ruggenthaler, M.; Appel, H.; Rubio, A. Atoms and Molecules in Cavities, from Weak to Strong Coupling in Quantum-Electrodynamics (QED) Chemistry. *Proc. Natl. Acad. Sci. U. S. A.* **2017**, *114*, 3026−3034.
(28) Shi, X.; Ueno, K.; Oshikiri, T.; Sun, Q.; Sasaki, K.; Misawa, H. Enhanced Water Splitting under Modal Strong Coupling Conditions. *Nat. Nanotechnol.* **2018**, *13*, 953−958.
(29) Fitzgerald, J. M.; Narang, P.; Craster, R. V.; Maier, S. A.; Giannini, V. Quantum Plasmonics. *Proc. IEEE* **2016**, *104*, 2307−2322.
(30) Bozhevolnyi, S. I.; Khurgin, J. B. The Case for Quantum Plasmonics. *Nat. Photonics* **2017**, *11*, 398−400.
(31) Wen, J.; Wang, H.; Wang, W.; Deng, Z.; Zhuang, C.; Zhang, Y.; Liu, F.; She, J.; Chen, J.; Chen, H.; et al. Room-Temperature Strong Light-Matter Interaction with Active Control in Single Plasmonic Nanorod Coupled with Two-Dimensional Atomic Crystals. *Nano Lett.* **2017**, *17*, 4689−4697.
(32) Stuhrenberg, M.; Munkhbat, B.; Baranov, D. G.; Cuadra, J.; Yankovich, A. B.; Antosiewicz, T. J.; Olsson, E.; Shegai, T. Strong Light-Matter Coupling between Plasmons in Individual Gold Bi-pyramids and Excitons in Mono- and Multilayer WSe_2. *Nano Lett.* **2018**, *18*, 5938−5945.
(33) Goncalves, P. A. D.; Bertelsen, L. P.; Xiao, S.; Mortensen, N. A. Plasmon-Exciton Polaritons in Two-Dimensional Semiconductor/metal Interfaces. *Phys. Rev. B: Condens. Matter Mater. Phys.* **2018**, *97*, 041402.
(34) Geisler, M.; Cui, X.; Wang, J.; Rindzevicius, T.; Gammelgaard, L.; Jessen, B. S.; Goncalves, P. A. D.; Todisco, F.; Bøggild, P.; Boisen, A.; Wubs, M.; Mortensen, N. A.; Xiao, S.; Stenger, N. Single-Crystalline Gold Nanodisks on WS_2 Mono- and Multilayers for Strong Coupling at Room Temperature. *ACS Photonics* **2019**, *6*, 994−1001.
(35) Yankovich, A. B.; Munkhbat, B.; Baranov, D. G.; Cuadra, J.; Olsén, E.; LourençoMartins, H.; Tizei, L. H.; Kociak, M.; Olsson, E.; Shegai, T. Visualizing Spatial Variations of Plasmon-Exciton Polaritons at the Nanoscale Using Electron Microscopy. *Nano Lett.* **2019**, *19*, 8171−8181.
(36) Lepeshov, S.; Wang, M.; Krasnok, A.; Kotov, O.; Zhang, T.; Liu, H.; Jiang, T.; Korgel, B.; Terrones, M.; Zheng, Y.; Alù, A. Tunable Resonance Coupling in Single Si Nanoparticle-Monolayer WS_2 Structures. *ACS Appl. Mater. Interfaces* **2018**, *10*, 16690−16697.
(37) Zakharko, Y.; Graf, A.; Zaumseil, J. Plasmonic Crystals for Strong Light-Matter Coupling in Carbon Nanotubes. *Nano Lett.* **2016**, *16*, 6504−6510.
(38) Graf, A.; Held, M.; Zakharko, Y.; Tropf, L.; Gather, M. C.; Zaumseil, J. Electrical Pumping and Tuning of Exciton-Polaritons in Carbon Nanotube Microcavities. *Nat. Mater.* **2017**, *16*, 911−917.
(39) Qian, C.; Wu, S.; Song, F.; Peng, K.; Xie, X.; Yang, J.; Xiao, S.; Steer, M. J.; Thayne, I. G.; Tang, C.; et al. Two-Photon Rabi Splitting

https://doi.org/10.1021/acs.nanolett.1c02248
Nano Lett. 2021, 21, 8979−8986

in a Coupled system of a Nanocavity and Exciton Complexes. *Phys. Rev. Lett.* **2018**, *120*, 213901.
(40) Cuadra, J.; Baranov, D. G.; Wersall, M.; Verre, R.; Antosiewicz, T. J.; Shegai, T. Observation of Tunable Charged Exciton Polaritons in Hybrid Monolayer WS_2-Plasmonic Nanoantenna System. *Nano Lett.* **2018**, *18*, 1777−1785.
(41) Törmä, P.; Barnes, W. l. Strong Coupling between SurfacePlasmon Polaritons and Emitters: a Review. *Rep. Prog. Phys.* **2015**, *78*, 013901.
(42) Tang, Y.; Gu, J.; Liu, S.; Watanabe, K.; Taniguchi, T.; Hone, J.; Mak, K. F.; Shan, J. Tuning Layer-Hybridized moiré Excitons by the Quantum-Confined Stark Effect. *Nat. Nanotechnol.* **2021**, *16*, 52−57.
(43) Zhou, Z.-K.; Liu, J.; Bao, Y.; Wu, L.; Png, C. E.; Wang, X.-H.; Qiu, C.-W. Quantum Plasmonics Get Applied. *Prog. Quantum Electron.* **2019**, *65*, 1−20.
(44) Baranov, D. G.; Wersäll, M.; Cuadra, J.; Antosiewicz, T. J.; Shegai, T. Novel Nanostructures and Materials for Strong Light-Matter Interactions. *ACS Photonics* **2018**, *5*, 24−42.
(45) Yi, Y.; Chen, Z.; Yu, X. F.; Zhou, Z. K.; Li, J. Recent Advances in Quantum Effects of 2D Materials. *Adv. Quant. Technol.* **2019**, *2*, 1800111.
(46) Zhong, X.; Chervy, T.; Zhang, L.; Thomas, A.; George, J.; Genet, C.; Hutchison, J. A.; Ebbesen, T. W. Energy Transfer between Spatially Separated Entangled Molecules. *Angew. Chem., Int. Ed.* **2017**, *56*, 9034−9038.
(47) Trivedi, R.; Radulaski, M.; Fischer, K. A.; Fan, S.; Vuckovic, J. Photon Blockade in Weakly Driven Cavity Quantum Electrodynamics Systems with Many Emitters. *Phys. Rev. Lett.* **2019**, *122*, 243602.
(48) Weber, J. H.; Kettler, J.; Vural, H.; Muller, M.; Maisch, J.; Jetter, M.; Portalupi, S. L.; Michler, P. Overcoming Correlation Fluctuations in Two-Photon Interference Experiments with Differently Bright and Independently Blinking Remote Quantum Emitters. *Phys. Rev. B: Condens. Matter Mater. Phys.* **2018**, *97*, 195414.
(49) Patel, R. B.; Bennett, A. J.; Farrer, I.; Nicoll, C. A.; Ritchie, D. A.; Shields, A. J. Two Photon Interference of the Emission from Electrically Tunable Remote Quantum dots. *Nat. Photonics* **2010**, *4*, 632−635.
(50) Srivastava, A.; Sidler, M.; Allain, A. V.; Lembke, D. S.; Kis, A.; Imamoglu, A. Optically Active Quantum Dots in Monolayer WSe_2. *Nat. Nanotechnol.* **2015**, *10*, 491−496.
(51) Chen, B.; Wei, Y.; Zhao, T.; Liu, S.; Su, R.; Yao, B.; Yu, Y.; Liu, J.; Wang, X. Bright Solid-State Sources for Single Photons with Orbital Angular Momentum. *Nat. Nanotechnol.* **2021**, *16*, 302−307.
(52) Bao, Y.; Lin, Q.; Su, R.; Zhou, Z.-K.; Song, J.; Li, J.; Wang, X.-H. On-Demand Spin-State Manipulation of Single-Photon Emission from Quantum Dot Integrated with Metasurface. *Sci. Adv.* **2020**, *6*, No. eaba876.

https://doi.org/10.1021/acs.nanolett.1c02248
Nano Lett. 2021, 21, 8979−8986